



TECHNICAL ARTICLE

A Novel Hypoeutectic High-Entropy Alloy $\text{CrFe}_2\text{Ni}_2\text{Mo}_{0.3}\text{Nb}_{0.25}$ with High Tensile Strength and Good Ductility

Wandong Wu, Weizhong Liang, Sheng Guan, Ransong Wei, and Zhiliang Ning

Submitted: 24 September 2021 / Revised: 8 February 2022 / Accepted: 4 March 2022 / Published online: 13 April 2022

In this paper, a new $\text{CrFe}_2\text{Ni}_2\text{Mo}_{0.3}\text{Nb}_x$ (x values in molar ratio, $x = 0, 0.25, 0.5, 0.75$) eutectic high-entropy alloy (EHEA) family was prepared to investigate the effect of intermetallic compounds upon its microstructure and tensile properties. The microstructure evolved from an initial single-phase FCC solid solution structure ($x=0$) to a hypoeutectic microstructure ($x = 0.25$), then to a near-eutectic microstructure ($x = 0.5$) and finally to a hypereutectic microstructure ($x = 0.75$), where the lamellar eutectic structure consisted of a dual phase of FCC solid solution and C14-type Laves phase. The tensile test results showed that the C14-type Laves phase significantly affected the tensile properties of the EHEAs. With increase in element Nb, the ultimate tensile strength increased firstly and subsequently decreased till with 8.62 at.% ($x=0.5$) Nb addition. The $\text{CrFe}_2\text{Ni}_2\text{Mo}_{0.3}\text{Nb}_{0.25}$ hypoeutectic high-entropy alloy exhibited a well combination of the ultimate tensile strength (868MPa) and an appropriate ductility (17%), which can be attributed to the balance of FCC and Laves phase, the second-phase strengthening provided by Laves phase as well as the solid solution strengthening resulted from adding element Nb in FCC solid solution.

Keywords eutectic high-entropy alloys, eutectic microstructure, laves phase, tensile properties

1. Introduction

The design concept of traditional alloy was often based on single principle, that is, one element was the primary element of the alloys, which limited the variety of alloys. The high-entropy alloys (HEAs) have rapidly attracted tons of attention due to the breaking through of the traditional alloy design strategy (Ref 1–3). HEAs have many excellent properties due to the unique microstructures and four effects (Ref 4–11), such as soft magnetic properties of $\text{FeCoNi}(\text{AlSi})_{0.2}$ HEA (Ref 5), the outstanding wear resistance of $\text{Co}_{1.5}\text{CrFeNi}_{1.5}\text{Ti}$ and $\text{Al}_{0.2}\text{Co}_{1.5}\text{CrFeNi}_{1.5}$ HEAs (Ref 6), superconductivity of $\text{Ta}_{34}\text{Nb}_{33}\text{Hf}_8\text{Zr}_{14}\text{Ti}_{11}$ HEA (Ref 7), the excellent fatigue resistance of $\text{Al}_{0.5}\text{CoCrCuFeNi}$ HEA (Ref 8, 9), the outstanding mechanical properties at low temperature of CoCrFeNiMn and $\text{AlCoCrFeNi}_{2.1}$ HEAs (Ref 10, 11). So, these HEAs may have

potential applications in cutters, mold, magnetic materials and other fields (Ref 12). However, most HEAs exhibited inferior fluidity and castability, which made scholars doubt the production and application of high-entropy alloys at kilogram or even ton grade (Ref 13).

Recently, eutectic high-entropy alloys (EHEAs) are becoming a new research hot spot for improving fluidity and castability of HEAs and maintaining their excellent mechanical properties (Ref 14–21). The appearance of EHEAs provided the possibility for industrial scale ingots with good quality and high performance (Ref 22). Many EHEAs with excellent mechanical properties have been designed, such as $\text{Zr}_{0.45}\text{Nb}_{0.73}\text{Hf}_{0.52}\text{Ta}_{0.76}\text{CoCrFeNi}_{2.1}$ EHEAs (Ref 13), $\text{AlCoCrFeNi}_{2.1}$ EHEA (Ref 18), CrFeNi_2Al EHEA (Ref 23), $\text{CoCrFeNiNb}_{0.45}\text{Zr}_{0.55}\text{Hf}_{0.4}\text{Ta}_{0.4}$ EHEAs (Ref 24), $\text{Ni}_{30}\text{Co}_{30}\text{Cr}_{10}\text{Fe}_{10}\text{Al}_{18}\text{W}_2$ EHEA (Ref 25) and CoCrFeNiMnPb EHEA (Ref 26). Most of these EHEAs contained some intermetallic compounds. Previous studies have shown that intermetallic compounds had a strong influence on the tensile properties of usual traditional alloys (Ref 27, 28). The excess intermetallic compounds directly led to the embrittlement of the traditional alloys. So, the formation of intermetallic compounds should be avoided for most traditional alloys (Ref 29). However, few studies have systematically studied the effect of intermetallic compounds on the tensile properties of EHEAs.

In this paper, in order to investigate the effect of intermetallic compounds upon EHEAs, $\text{CrFe}_2\text{Ni}_2\text{Mo}_{0.3}\text{Nb}_x$ (x values in molar ratio, $x = 0.25, 0.50$ and 0.75) EHEA family with intermetallic compounds Laves phase was successfully prepared by adding Nb element in $\text{CrFe}_2\text{Ni}_2\text{Mo}_{0.3}$ HEA. The effects of Nb element and Laves phase on the microstructure and tensile properties of $\text{CrFe}_2\text{Ni}_2\text{Mo}_{0.3}\text{Nb}_x$ EHEAs were systematically investigated.

Wandong Wu, Weizhong Liang, Sheng Guan, and Ransong Wei, School of Materials Science and Engineering, Heilongjiang University of Science and Technology, Harbin 150022, People's Republic of China; Zhiliang Ning, School of Materials Science and Engineering, Harbin Institute of Technology, Harbin 150001, People's Republic of China. Contact e-mails: wzliang1966@126.com zhiliangning@sina.com.

2. Experimental

The button-shaped ingots of the alloys with the composition of $\text{CrFe}_2\text{Ni}_2\text{Mo}_{0.3}\text{Nb}_x$ (x values in molar ratio, $x=0, 0.25, 0.50$ and 0.75 , denoted as Nb0, Nb0.25, Nb0.5 and Nb0.75, respectively) were prepared by arc vacuum melting in a Ti-gettered argon atmosphere. The nominal purity of each element (Cr, Fe, Ni, Mo and Nb) is higher than 99.9%. In order to ensure the uniformity of composition, each ingot was re-melted six times. The cylindrical rods with a diameter of 9 mm and the length of 75 mm were fabricated by drop-casting into a copper mold.

The phase identification of the studied alloys was detected by a DX-2700B x-ray diffractometer (XRD) with $\text{Cu-K}\alpha$ radiation ($\lambda=1.5405\text{\AA}$), and the 2θ angle was from 20° to 100° with a scanning step of 0.02° . The thermal behavior analysis of the studied alloys was carried out by using a high-temperature differential scanning calorimeter (DSC) at a heating rate of 10K/min. The tensile tests of the studied alloys were performed on an AG-S plus tensile testing machine at a strain rate of $1.7 \times 10^{-3} \text{s}^{-1}$, where specimens for tensile tests were cut into dog-bone from each cylindrical rod by electro-discharge machining. The microstructures of the studied alloys were characterized by a QUANTA 200F scanning electron microscopy (SEM) with the energy-dispersive distribution (EDS). The volume fractions of the phases of the studied alloys were estimated by Image-pro Plus (IPP) software.

3. Results and Discussion

3.1 Phase Constitutions and Microstructures of $\text{CrFe}_2\text{Ni}_2\text{Mo}_{0.3}\text{Nb}_x$ Alloys

3.1.1 Phase Constitutions. Figure 1 shows the XRD patterns of the $\text{CrFe}_2\text{Ni}_2\text{Mo}_{0.3}\text{Nb}_x$ ($x=0, 0.25, 0.5$ and 0.75) alloys. It can be seen that the C14-type Fe_2Nb Laves phase (space group of P63/mmc, $a=b=4.813\text{\AA}$, $c=7.849\text{\AA}$) (Ref 30) and the FCC solid solution phase were clearly identified on the $\text{CrFe}_2\text{Ni}_2\text{Mo}_{0.3}\text{Nb}_x$ alloys patterns. With increase in element

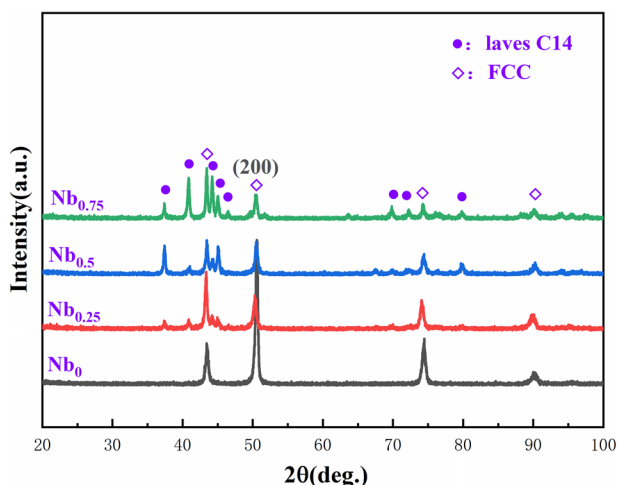


Fig. 1 The XRD patterns of the $\text{CrFe}_2\text{Ni}_2\text{Mo}_{0.3}\text{Nb}_x$ ($x=0, 0.25, 0.5$ and 0.75) alloys

Nb, the structure of the alloys changed from the simple FCC solid solution phase ($x = 0$) to a FCC+laves duplex phase ($x > 0$). The increase in diffraction peak intensity of the C14-type Laves phase showed its increase in volume fraction (Table 1). Besides, the peaks of FCC phase shifted slightly to lower diffraction angle (2θ) with increase in Nb, indicating the increase in its lattice parameters of FCC phase. The similar phenomenon was observed in other studies (Ref 22, 31, 32). According to the ΔH_{mix} (the mixing enthalpy), δ_r (the atomic radius difference) and VEC (valence electron concentration) thermo-physical parameters, which are closely related to Hume-Rothery's rule (Ref 33-38), the phases formation regularity can be inferred for the $\text{CrFe}_2\text{Ni}_2\text{Mo}_{0.3}\text{Nb}_x$ alloys. The values of VEC, δ_r and ΔH_{mix} were calculated for the $\text{CrFe}_2\text{Ni}_2\text{Mo}_{0.3}\text{Nb}_x$ alloys, as shown in Table 2. It can be concluded that the δ_r and ΔH_{mix} value ranges of the Nb0 alloy, which had a single phase, did agree with Zhang's criterion that a single-phase solid solution would form when $\delta_r \leq 4\%$ and $-15 \leq \Delta H_{\text{mix}} \leq 5$ kJ/mol in HEAs (Ref 33). The VEC value ranges of the Nb0 and Nb0.25 alloys, which had FCC solid solution phase, were consistent with Guo's criterion that FCC solid solution would form when VEC was greater than 8 (Ref 34). The Nb0.25, Nb0.5 and Nb0.75 alloys fully conformed to the rule of eutectic structure formation proposed by Barnasree chanda, i.e., it was propitious for the eutectic structure to become stable when $\delta_r > 3\%$, $-18 \leq \Delta H_{\text{mix}} \leq -6$ and $6 \leq \text{VEC} \leq 8.5$ (Ref 35). According to the XRD results, the observed phases conformed to the predictions by the thermo-physical parameters of the EHEA design.

3.1.2 Microstructures of the $\text{CrFe}_2\text{Ni}_2\text{Mo}_{0.3}\text{Nb}_x$ Alloys. Figure 2 shows the microstructures of the $\text{CrFe}_2\text{Ni}_2\text{Mo}_{0.3}\text{Nb}_x$ ($x=0, 0.25, 0.5$ and 0.75) alloys. It can be seen that a single dendritic morphology was observed in Nb0 alloy (Fig. 2a), which was consistent with its XRD pattern. The formation of dendritic morphology for the Nb0 alloy may be due to the non-equilibrium solidification, which was caused by the element Mo with a large atomic radius and high melting temperature during the solidification process (Ref 22). Regions enriched in element Mo tended to solidify firstly and formed dendrites (as marked by DR in Fig. 2a) due to the composition fluctuations, while regions containing less element Mo solidified later and formed interdendrites (as marked by ID in Fig. 2a) (Ref 22). The EDS results listed in Table 3 further proved the changes of Mo element in ID and DR regions. This similar phenomenon has appeared in other studies (Ref 22). With increase in element Nb, the Nb0.25, Nb0.5 and Nb0.75 alloys displayed the morphological characteristics of the different degree eutectic structure, as shown in Fig. 2(b), (c) and (d), respectively. The Nb0.25, Nb0.5 and Nb0.75 alloys were hypoeutectic, full near-eutectic and hypereutectic HEAs, respectively. The hypoeutectic structure of the Nb0.25 HEA consisted of a primary FCC solid solution structure (as marked

Table 1 The volume fraction of the FCC phase and C14-type Laves phase

Alloys, %	Nb0	Nb0.25	Nb0.5	Nb0.75
FCC	100	82.6	52.7	31.7
Laves	0	17.4	47.3	68.3

by A in Fig. 2b) and lamellar eutectic structure. The amplificatory image of the square region was shown in inset; the lamellar eutectic structure was marked by E in Fig. 2(b) inset. The full near-eutectic structure of the Nb0.5 alloy (Fig. 2c) was similar to the microstructures of the several reported typical EHEAs (Ref 39-43). The amplificatory image of the square region was shown in Fig. 2(c) inset. A primary C14-type Laves phase (as marked by B in Fig. 2d) and lamellar eutectic structure were present in the hypereutectic structure of Nb0.75 HEA. The amplificatory image of the square region is shown in Fig. 2(d) inset. The observed eutectic structure of Nb0.25, Nb0.5 and Nb0.75 HEAs conformed to the expectant EHEA family design.

Figure 3 shows the DSC curves of the $\text{CrFe}_2\text{Ni}_2\text{Mo}_{0.3}\text{Nb}_x$ ($x=0, 0.25, 0.5$ and 0.75) alloys. It can be seen that the Nb0 alloy only had one endothermic peak, in agreement with its single-phase FCC solid solution structure. With increase in element Nb, a sharp endothermic peak appeared on the Nb0.5 alloy DSC curve, proving the near-full eutectic structure of the Nb0.5 alloy (Ref 22). Two distinct endothermic peaks were observed on the Nb0.25 and Nb0.75 alloys DSC

Table 2 Calculated parameters (ΔH_{mix} , δr , VEC) of the $\text{CrFe}_2\text{Ni}_2\text{Mo}_{0.3}\text{Nb}_x$ ($x=0, 0.25, 0.5$ and 0.75) alloys

Alloys	ΔH_{mix} , kJ/mol	Δr , %	VEC
Nb0	- 3.75	2.71	8.26
Nb0.25	- 7.09	3.85	8.12
Nb0.5	- 9.49	5.01	7.98
Nb0.75	- 11.47	5.61	7.85

Table 3 The chemical compositions of different regions in the $\text{CrFe}_2\text{Ni}_2\text{Mo}_{0.3}\text{Nb}_x$ ($x=0, 0.25, 0.5$ and 0.75) alloys

Alloys	Regions	Chemical compositions/at.%				
		Cr	Fe	Ni	Mo	Nb
Nb0	DR	17.52	34.83	37.69	9.96	...
	IR	16.32	37.40	39.78	6.5	...
Nb0.25	A	18.63	38.81	37.23	3.96	1.37
	E	17.21	32.62	35.27	6.64	8.26
Nb0.5	E	14.66	32.35	34.59	7.95	10.44
Nb0.75	B	15.07	33.10	24.95	7.23	19.65
	E	18.07	35.49	35.84	3.53	7.08

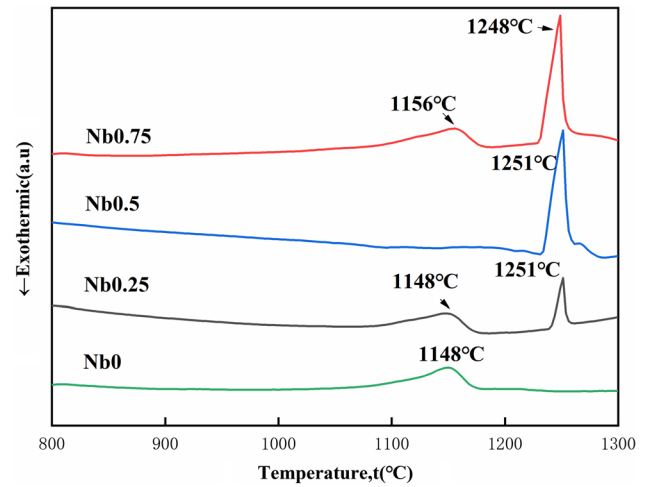


Fig. 3 The DSC curves of the $\text{CrFe}_2\text{Ni}_2\text{Mo}_{0.3}\text{Nb}_x$ ($x=0, 0.25, 0.5$ and 0.75) alloys

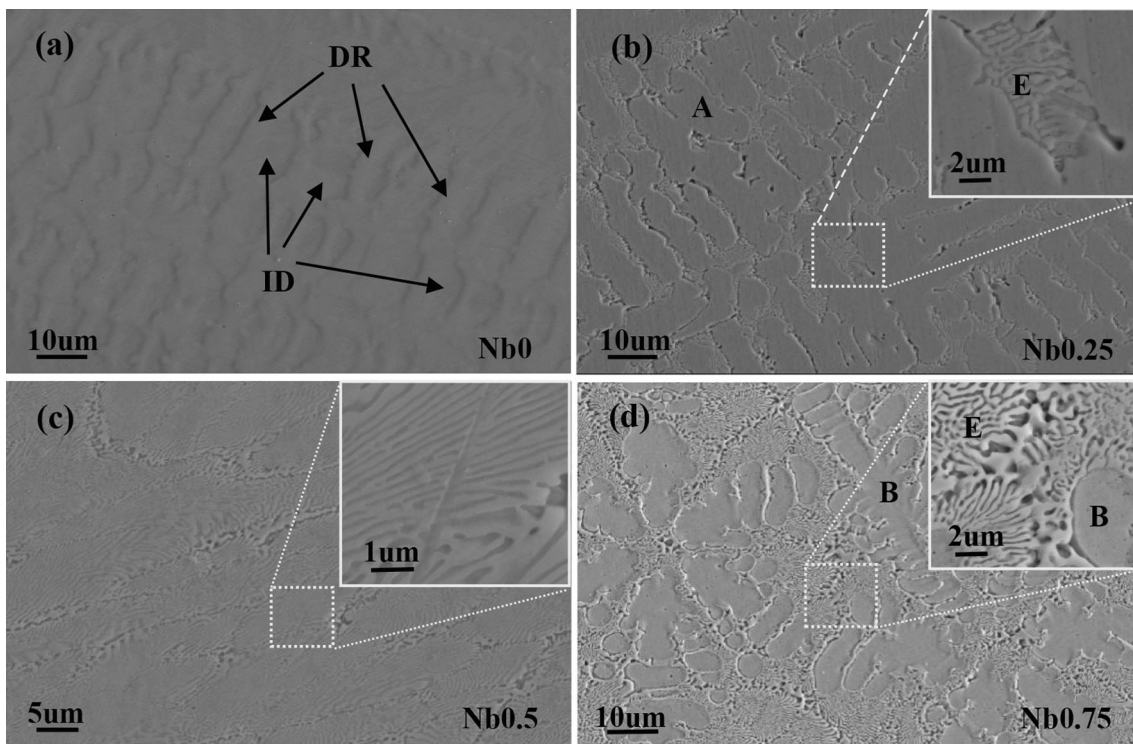


Fig. 2 The microstructures of the $\text{CrFe}_2\text{Ni}_2\text{Mo}_{0.3}\text{Nb}_x$ alloys: (a) $x=0$ (b) $x=0.25$; (c) $x=0.5$; (d) $x=0.75$

curves, respectively. When combined with the primary FCC phase + eutectic structure of Nb0.25 alloy and the primary Fe₂Nb Laves phase + eutectic structure of Nb0.75 alloy, it can be concluded that the Nb0.25 and Nb0.75 HEAs were hypoeutectic and hypereutectic HEAs, respectively (Ref 22, 25).

Figure 4 shows the EDS maps of the CrFe₂Ni₂Mo_{0.3}Nb_x (x=0, 0.25, 0.5 and 0.75) alloys, giving a vivid presentation of element distribution in the alloys. The EDS results are shown in Table 3. In the Nb0 alloy, the constituent elements Ni, Cr and

Fe were distributed uniformly except for element Mo, where region DR was enriched in element Mo. This may be due to the large atomic radius difference and negative mixing enthalpy between Mo and the other elements Cr, Fe and Ni. For the Nb0.5 alloy, all the constituent elements were distributed uniformly. For the Nb0.25 and Nb0.75 alloys, it was clear that the constituent elements Ni, Cr and Fe were still distributed uniformly except for elements Mo and Nb. The region E (eutectic structure, Nb0.25 alloy) and region B (the primary C14-type Fe₂Nb Laves phase, Nb0.75 alloy) were enriched in

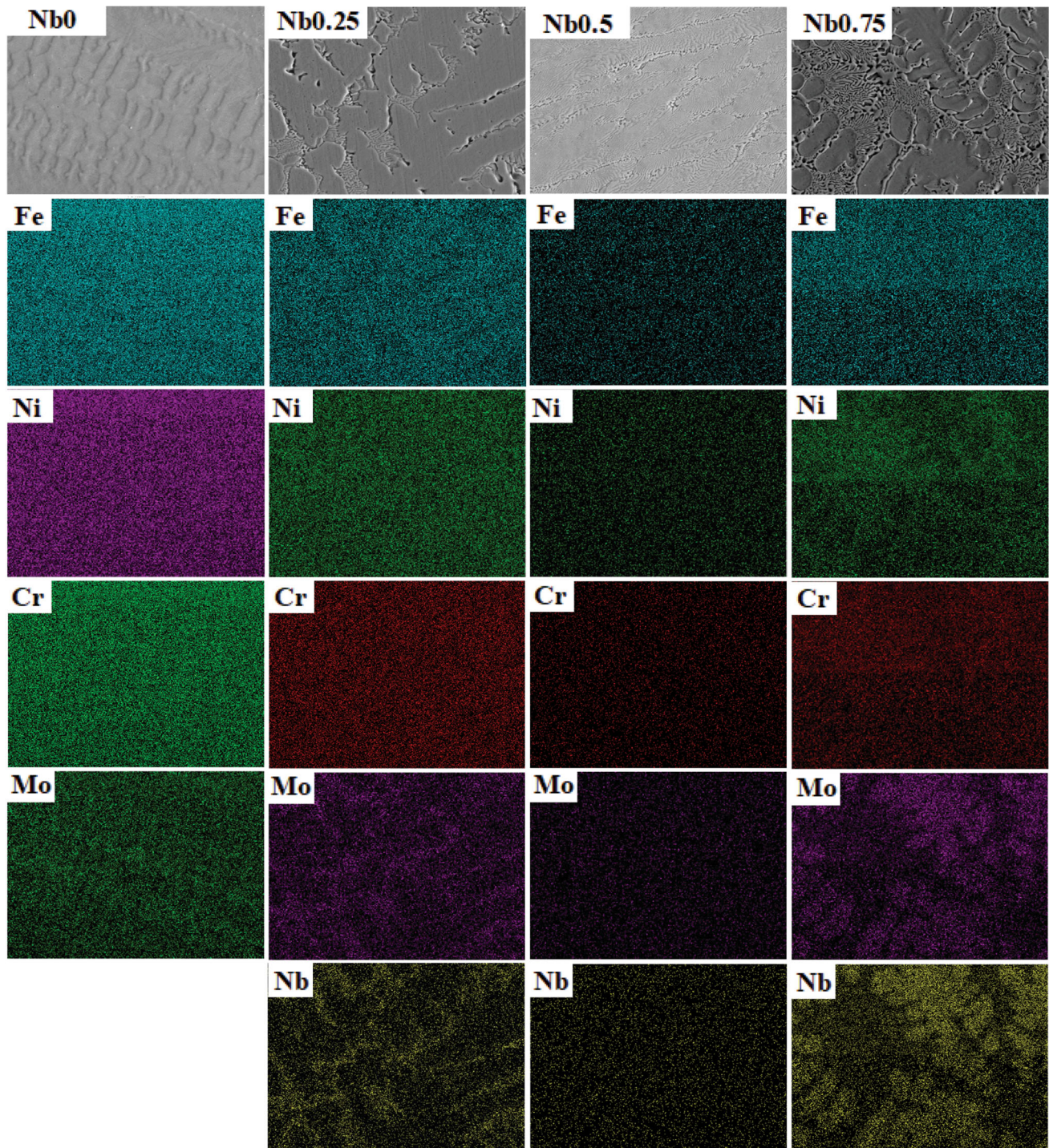


Fig. 4 The EDS maps of the CrFe₂Ni₂Mo_{0.3}Nb_x (x=0, 0.25, 0.5 and 0.75) alloys

Nb and Mo element, further proving correctness of the analysis of their XRD patterns.

3.2 Mechanical Properties and Fracture Behaviors

Figure 5 shows the tensile stress–strain curves of the $\text{CrFe}_2\text{Ni}_2\text{Mo}_{0.3}\text{Nb}_x$ ($x=0, 0.25, 0.5$ and 0.75) alloys. With increase in element Nb, the ultimate tensile strength increased firstly and subsequently decreased till with 8.62 at.% ($x=0.5$) Nb addition. The Nb0 alloy exhibited excellent ductility, the tensile strain reached $\sim 67\%$, and the yield strength and ultimate tensile strength were 244 MPa and 549 MPa, respectively. The lower strength of the Nb0 alloy was due to no alloying effects of Nb element and its solution strengthening (Ref 22). With adding element Nb, the Nb0.25 alloy exhibited the most excellent comprehensive tensile properties, the yield strength and ultimate tensile strength were up to 533 MPa and 868 MPa, respectively, and tensile strain was up to $\sim 17\%$. By combining the results of XRD (Fig. 1), SEM (Fig. 2) and the volume fraction of the FCC phase and C14-type Laves phase (Table 1), it was reasonable to infer the reasons for the improvement of the tensile properties of the Nb0.25 alloy. During the tensile deformation process, initially, the hard and brittle C14-type Laves phase and the soft FCC solid solution underwent elastic deformation; then, the soft FCC solid solution was elongated and deformed while the hard C14-type Laves phase was barely deformed, resulting in a mechanical incompatibility. Therefore, further deformation of the plastic deforming soft regions was restricted, leading to the formation of the gradients of plastic strain between the deforming soft region and eutectic structure (FCC+C14-type Laves phase), which required geometrically necessary dislocations (GNDs) to deform further, which was helpful to the promotion of the strength of the Nb0.25 alloy (Ref 29). Apart from GNDs, the second-phase strengthening provided by the C14-type Laves phase, as well as the solid solution strengthening resulted from the additions of element Nb in FCC solid solutions, also made contributions to the promotion of the strength.

With further adding element Nb, for the Nb0.5 and Nb0.75 alloys, a prominent decrease in both ductility and ultimate tensile strength appeared. The reason why a prominent decrease in both ductility and strength of the Nb0.5 and Nb0.75 alloys

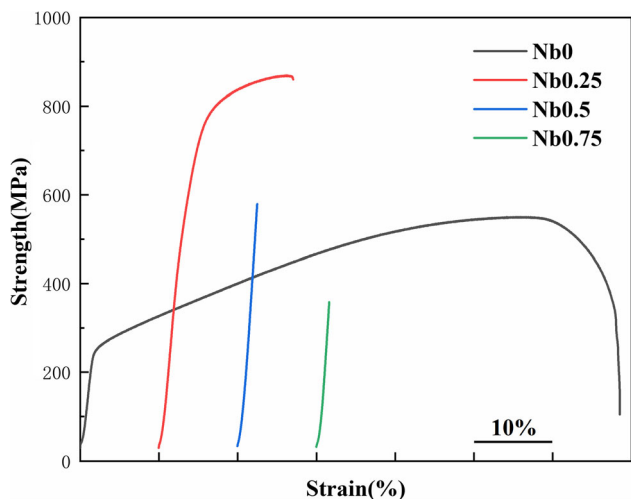


Fig. 5 The tensile properties of the $\text{CrFe}_2\text{Ni}_2\text{Mo}_{0.3}\text{Nb}_x$ alloys: $x = 0$; $x = 0.25$; $x = 0.5$; $x = 0.75$

may be the embrittlement which led by excess C14-type Laves phase (Ref 44). With increase in element Nb, the volume fraction of the C14-type Laves phase increased (table 1). This indicated that the C14-type Laves phase significantly affected the tensile properties of the two alloys. That meant that the Nb0.5 and Nb0.75 alloys might fracture before the fracture strength reached its ideal value because of the embrittlement which led by excess C14-type Laves phase (Ref 44, 45). In a word, for the $\text{CrFe}_2\text{Ni}_2\text{Mo}_{0.3}\text{Nb}_x$ ($x=0.25, 0.5$ and 0.75) alloys, when the content of C14-type Laves phase (Nb0.25 alloy) was low, the EHEA at these hypoeutectic states was still dominated by the FCC solid solution phase, so the strength of the EHEAs can be significantly improved by GNDs, the second-phase strengthening and the solid solution strengthening under the premise of maintaining a high ductility (Ref 29). With increase in the C14-type Laves phase content (Nb0.5~Nb0.75 EHEAs), the alloys were dominated by the hard and brittle Laves phase, and became rapidly brittle and the strength and ductility decreased sharply (Ref 44).

The tensile properties (ultimate tensile strength (UTS) and elongation (E_f)) of as-cast Nb-added Laves intermetallic containing EHEAs (in our study) are compared with other selected Nb-added Laves intermetallic containing EHEAs and HEAs in Fig. 6 (Ref 28, 46-48). It is observed that the as-cast $\text{CrFe}_2\text{Ni}_2\text{Mo}_{0.3}\text{Nb}_{0.25}$ hypoeutectic high-entropy alloy has better comprehensive tensile properties than other as-cast Nb-added Laves intermetallic containing HEAs. However, compared with the Nb-added Laves intermetallic containing HEAs which have undergone aging or thermomechanical treatments, there is a gap in tensile mechanical properties, which has also provided inspiration for our subsequent research to improve the mechanical properties of the EHEAs we designed by aging and thermomechanical treatments.

The tensile fracture surface morphologies of the $\text{CrFe}_2\text{Ni}_2\text{Mo}_{0.3}\text{Nb}_x$ ($x = 0, 0.25, 0.5$ and 0.75) alloys are shown in Fig. 7. The fracture surface of the Nb0 alloy presented mainly dimples (see Fig. 7a), indicating a ductile fracture mode, which was consistent with the excellent ductility of the Nb0 alloy. With increase in element Nb, for the Nb0.25 alloy, the number of

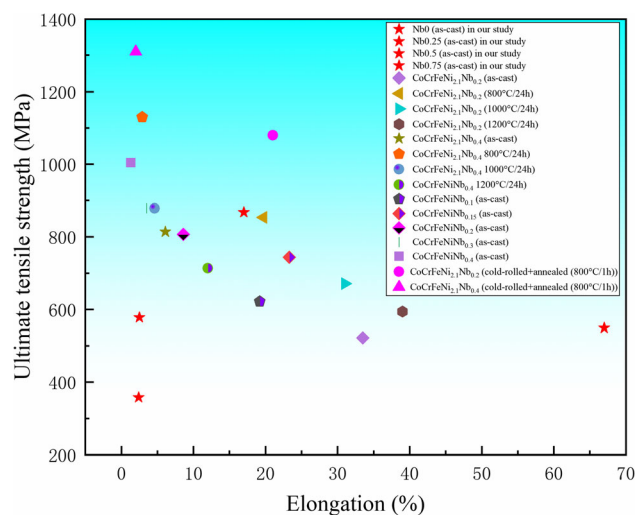


Fig. 6 The tensile properties of as-cast Nb-added Laves intermetallic containing EHEAs (in our study) are compared with other selected Nb-added Laves intermetallic containing EHEAs and HEAs in the ultimate tensile strength versus Elongation plot

dimples decreased sharply and the fracture surface exhibited tearing ridges and many trenches, where the trenches mainly formed in the eutectic structure region (Fig. 7b). By connecting the primary FCC phase + eutectic structure from the results of XRD (Fig. 1) and SEM (Fig. 2), the formation of trenches morphologies can be explained reasonably: during tensile process, the soft FCC phase was elongated and deformed, while the hard and brittle Laves phase was barely deformed, resulting in the undeformed hard and brittle Laves phase forming the bottom of the trenches while the stretched thin layer FCC phase forming the two edges of the trenches (Ref 11). The decrease in dimples, the formation and inhomogeneous distribution of trenches directly led to the decrease in the ductility of the Nb0.25 alloy. For the Nb0.5 alloy, the dimples disappeared completely, the fracture feature of the Nb0.5 alloy was mainly trenches (Fig. 7c), suggesting a brittle fracture mode, which was consistent with the inferior ductility of the Nb0.5 alloy. The reason why the fracture surface was filled with trenches was that the Nb0.5 alloy was a full near-eutectic structure. With further increase in Nb content, for the Nb0.75 alloy, most of the trenches were replaced by the large and irregular plane of the primary C14-type Laves phase, further proving that, during the tensile deformation process, the soft FCC phase deformed, while the hard and brittle C14-type Laves phase was directly broken without deforming. The inhomogeneous distribution of the large and irregular Laves phase can lead to the stress concentration at the phase interface between Laves phase and eutectic structure, and it is easy to fracture at the phase interface during the tensile process.

4. Conclusions

In this work, $\text{CrFe}_2\text{Ni}_2\text{Mo}_{0.3}\text{Nb}_x$ ($x = 0, 0.25, 0.50$ and 0.75) EHEAs were prepared. The effects of the addition of element Nb and C14-type Laves phase on microstructures and tensile properties of the $\text{CrFe}_2\text{Ni}_2\text{Mo}_{0.3}\text{Nb}_x$ EHEAs were investigated; the conclusions were as follows:

- 1) For the $\text{CrFe}_2\text{Ni}_2\text{Mo}_{0.3}\text{Nb}_x$ EHEAs, with increase in element Nb, the microstructure evolved from an initial single-phase FCC solid solution structure ($x = 0$) to a hypoeutectic microstructure ($0.25 < x < 0.5$), then to a full near-eutectic ($x = 0.5$), and finally to a hypereutectic microstructure ($x > 0.75$).
- 2) The $\text{CrFe}_2\text{Ni}_2\text{Mo}_{0.3}$ HEA exhibited a good ductility, the tensile strain was up to 67%, the $\text{CrFe}_2\text{Ni}_2\text{Mo}_{0.3}\text{Nb}_{0.25}$ hypoeutectic HEA exhibited an excellent combination of ductility and strength, the ultimate tensile strength was up to 868 MPa, and the tensile strain was up to ~17%. For the $\text{CrFe}_2\text{Ni}_2\text{Mo}_{0.3}\text{Nb}_{0.5}$ eutectic HEA and $\text{CrFe}_2\text{Ni}_2\text{Mo}_{0.3}\text{Nb}_{0.75}$ hypereutectic HEA, the ultimate tensile strength was 578, 358 MPa and the tensile strain was 2.5, 1.6%, respectively.
- 3) The content of C14-type Laves phase had a significant effect on the tensile properties of the $\text{CrFe}_2\text{Ni}_2\text{Mo}_{0.3}\text{Nb}_x$ ($x = 0, 0.25, 0.50$ and 0.75) EHEAs. A proper amount of Laves phase can greatly improve the strength and maintain an appropriate ductility in $\text{CrFe}_2\text{Ni}_2\text{Mo}_{0.3}\text{Nb}_{0.25}$ hypoeutectic high-entropy alloy, which can be attributed

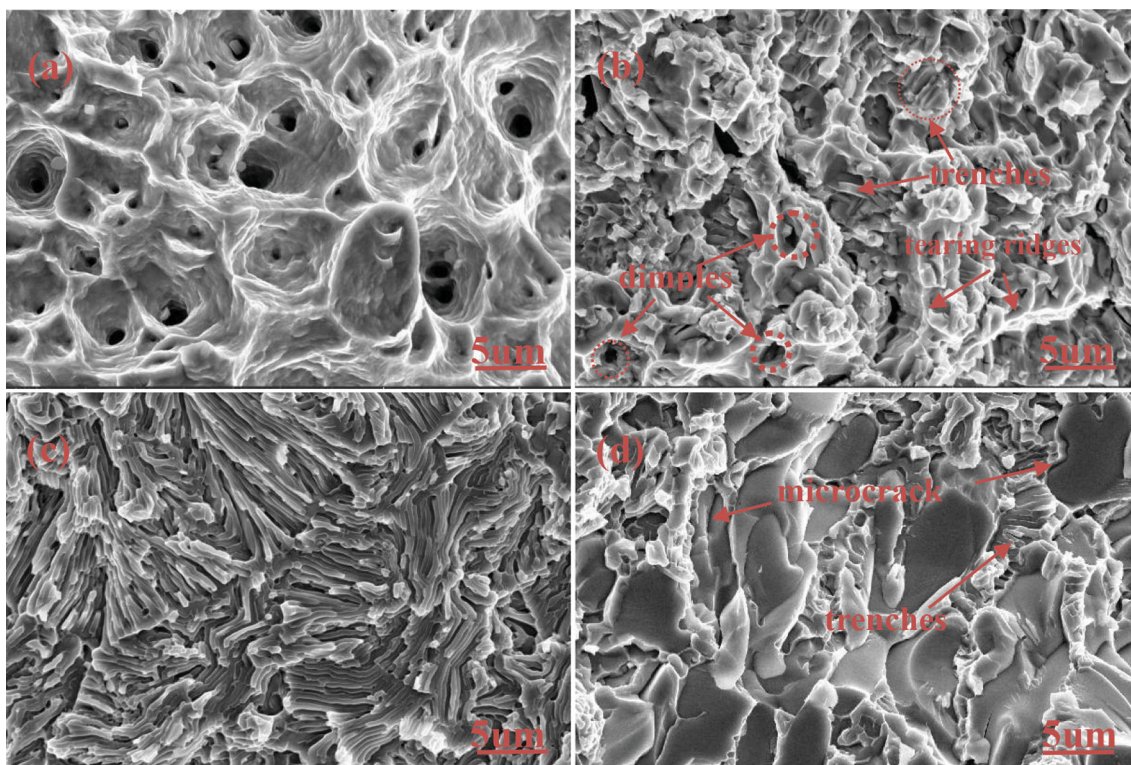


Fig. 7 The tensile fracture surface morphologies of the $\text{CrFe}_2\text{Ni}_2\text{Mo}_{0.3}\text{Nb}_x$ alloys: (a) $x = 0$; (b) $x = 0.25$; (c) $x = 0.5$; (d) $x = 0.75$

to the balance of FCC and Laves phase, the second-phase strengthening provided by Laves phase as well as the solid solution strengthening resulted from adding element Nb in FCC solid solution.

Acknowledgments

This work was supported by the National Natural Science Foundation of China (Grant No. 52171155 and 52071118) and the Graduate Innovation Research Fund Project of Heilongjiang University of Science and Technology (Grant YJSCX2021-212HKD).

Author contributions

All authors contributed to the study. The experiment and data collection were performed by WDW, SG and RSW. The experiment data analysis was performed by WDW, WZL and ZLN. The first draft of the manuscript was written by WDW and WZL, and the draft was supervised by WZL and ZLN. All authors read and approved the final manuscript.

Conflict of interest

This is the first submission of this manuscript and no parts of this manuscript are being considered for publication elsewhere. All authors have approved this manuscript. No author has financial or other contractual agreements that might cause conflicts of interest.

References

1. B. Cantor, I.T.H. Chang, P. Knight and A.J.B. Vincent, Microstructural Development in Equiatomic Multicomponent Alloys, *Mat. Sci. Eng. A*, 2004, **375–377**, p 213–218.
2. J.W. Yeh, S.K. Chen, S.J. Lin, J.Y. Gan, T.S. Chin, T.T. Shun, C.H. Tsau and S.Y. Chang, Nanostructured High-Entropy Alloys with Multiple Principal Elements: Novel Alloy Design Concepts and Outcomes, *Adv. Eng. Mater.*, 2004, **6**(5), p 299–303.
3. Y.P. Lu, Y. Dong, H. Jiang, Z.J. Wang, Z.Q. Cao, S. Guo, T.M. Wang, T. Li and P.K. Liaw, Promising Properties and Future Trend of Eutectic High Entropy Alloys, *Scr. Mater.*, 2020, **187**, p 202–209.
4. Y.P. Lu, Y. Dong, S. Guo, L. Jiang, H. Kang, T. Wang, B. Wen, Z.J. Wang, J.C. Jie, Z.Q. Cao, H.H. Ruan and T.J. Li, A Promising New Class of High-Temperature Alloys: Eutectic High-Entropy Alloys, *Sci. Rep.*, 2014, **4**, p 6200.
5. Y. Zhang, T.T. Zuo, Y.Q. Cheng and P.K. Liaw, High-Entropy Alloys with High Saturation Magnetization, Electrical Resistivity, and Malleability, *Sci. Rep.*, 2013, **3**, p 1455.
6. M.H. Chuang, M.H. Tsai, W.R. Wang, S.J. Lin and J.W. Yeh, Microstructure and Wear Behavior of $\text{Al}_{0.5}\text{Co}_{1.5}\text{CrFeNi}_{1.5}\text{Ti}_y$ high-Entropy Alloys, *Acta Mater.*, 2011, **59**(16), p 6308–6317.
7. P. Kozelj, S. Vrtnik, A. Jelen, S. Jazbec, Z. Jaglicic, S. Maiti, M. Feuerbacher, W. Steurer and J. Dolinsek, Discovery of a Super Conducting High-Entropy Alloy, *Phys. Rev. Lett.*, 2014, **113**, p 107001.
8. M.A. Hemphill, T. Yuan, G.Y. Wang, J.W. Yeh, C.W. Tsai, A. Chuang and P.K. Liaw, Fatigue Behavior of $\text{Al}_{0.5}\text{CoCrCuFeNi}$ High Entropy Alloys, *Acta Mater.*, 2012, **60**(16), p 5723–5734.
9. Z. Tang, T. Yuan, C.W. Tsai, J.W. Yeh, C.D. Lundin and P.K. Liaw, Fatigue Behavior of a Wrought $\text{Al}_{0.5}\text{CoCrCuFeNi}$ Two-Phase High-Entropy Alloy, *Acta Mater.*, 2015, **99**, p 247–258.
10. B. Gludovatz, A. Hohenwarter, D. Catoor, E.H. Chang, E.P. George and R.O. Ritchie, A Fracture-Resistant High-Entropy Alloy for Cryogenic Applications, *Science*, 2014, **345**, p 1153–1158.
11. Y.P. Lu, X.Z. Gao, L. Jiang, Z.N. Chen, T.M. Wang, J.C. Jie, H.J. Kang, Y.B. Zhang, S. Guo, H.H. Ruan, Y.H. Zhao, Z.Q. Cao and T.J. Li, Directly Cast Bulk Eutectic and Near-Eutectic High Entropy Alloys with Balanced Strength and Ductility in a Wide Temperature Range, *Acta Mater.*, 2017, **124**, p 143–150.
12. Y. Zhang, T.T. Zuo, Z. Tang, M.C. Gao, K.A. Dahmen, P.K. Liaw and Z.P. Lu, Microstructures and Properties of High-Entropy Alloys, *Prog. Mater. Sci.*, 2014, **61**, p 1–93.
13. Y.P. Lu, H. Jiang, S. Guo, T.M. Wang, Z.Q. Cao and T.J. Li, A New Strategy to Design Eutectic High-Entropy Alloys using Mixing Enthalpy, *Intermetallics*, 2017, **91**, p 124–128.
14. M.L. Wang, Y.P. Lu, T.M. Wang, T.J. Li and P.K. Liaw, A Novel Bulk Eutectic High-Entropy Alloy with Outstanding as-cast Specific Yield Strengths at Elevated Temperatures, *Scr. Mater.*, 2021, **204**, p 114–132.
15. L.L. Han, X.D. Xu, Z.M. Li, B. Liu and Y. Liu, A Novel Equiaxed Eutectic High-Entropy Alloy With Excellent Mechanical Properties at Elevated Temperatures, *Mater. Res. Lett.*, 2020, **8**(10), p 373–382.
16. W. Huo, H. Zhou, F. Fang, Z. Xie and J. Jiang, Microstructure and Mechanical Properties of CoCrFeNiZr_x Eutectic High-Entropy Alloys, *Mater. Design.*, 2017, **134**, p 226–233.
17. T. Bhattacharjee, I.S. Wani, S. Sheikh, I.T. Clark, T. Okawa, S. Guo, P.P. Bhattacharjee and N. Tsuji, Simultaneous Strength-Ductility Enhancement of a Nano-Lamellar $\text{AlCoCrFeNi}_{2.1}$ Eutectic High Entropy Alloy by Cryo-Rolling and Annealing, *Sci. Rep.*, 2018, **8**(1), p 1–8.
18. I.S. Wani, T. Bhattacharjee, S. Sheikh, P.P. Bhattacharjee, S. Guo and N. Tsuji, Tailoring Nanostructures and Mechanical Properties of $\text{AlCoCrFeNi}_{2.1}$ Eutectic High Entropy Alloy Using Thermo-Mechanical Processing, *Mater. Sci. Eng. A*, 2016, **675**, p 99–109.
19. S.R. Reddy, S. Yoshida, U. Sunkari, A. Lozinko, J. Joseph, R. Saha, D. Fabijanic, S. Guo, P.P. Bhattacharjee and N. Tsuji, Engineering Heterogeneous Microstructure by Severe Warm-Rolling for Enhancing Strength-Ductility Synergy in Eutectic High Entropy Alloys, *Mater. Sci. Eng. A*, 2019, **764**, p 138226.
20. S.R. Reddy, S. Yoshida, T. Bhattacharjee, N. Snake, A. Lozinko, S. Guo, P.P. Bhattacharjee and N. Tsuji, Nanostructuring with Structural-Compositional Dual Heterogeneities Enhances Strength-Ductility Synergy in Eutectic High Entropy Alloy, *Sci. Rep.*, 2019, **9**, p 11505.
21. B. Tripathy, S.R.K. Malladi and P.P. Bhattacharjee, Development of Ultrafine Grained Cobalt-Free $\text{AlCrFe}_2\text{Ni}_2$ High Entropy Alloy With Superior Mechanical Properties by Thermo-Mechanical Processing, *Mater. Sci. Eng. A*, 2021, **831**, p 142190.
22. W.N. Jiao, H. Jiang, D.X. Qiao, J.Y. He, H.L. Zhao, Y.P. Lu and T.J. Li, Effects of Mo on Microstructure and Mechanical Properties of $\text{Fe}_2\text{Ni}_2\text{CrMox}$ Eutectic High Entropy Alloys, *Mater. Chem. Phys.*, 2021, **260**, p 124175.
23. X. Jin, J. Bi, L. Zhang, Y. Zhou, X.Y. Du, Y.X. Liang and B.S. Li, A New CrFeNi_2Al Eutectic High Entropy Alloy System with Excellent Mechanical Properties, *J. Alloy. Compd.*, 2019, **770**, p 655–661.
24. H. Jiang, K.M. Han, X.X. Gao, Y.P. Lu, Z.Q. Cao, M.C. Gao, J.A. Hawk and T.J. Li, A New Strategy to Design Eutectic High-Entropy Alloys Using Simple Mixture Method, *Mater. Des.*, 2018, **142**, p 101–105.
25. Q.F. Wu, Z.J. Wang, T. Zheng, D. Chen, Z.S. Yang, J.J. Li, J.J. Kai and J.C. Wang, A Casting Eutectic High Entropy Alloy With Superior Strength-Ductility Combination, *Mater. Lett.*, 2019, **253**, p 268–271.
26. Y.M. Tan, J.S. Li, J. Wang and H.C. Kou, Seaweed Eutectic-Dendritic Solidification Pattern in a CoCrFeNiMnPd Eutectic High-Entropy Alloy, *Intermetallics*, 2017, **85**, p 74–79.
27. W.H. Liu, Z.P. Liu, J.Y. He, J.H. Luan, Z.J. Wang, B. Liu, Y. Liu, M.W. Chen and C.T. Liu, Ductile CoCrFeNiMox High Entropy Alloys Strengthened by Hard Intermetallic Phases, *Acta Mater.*, 2016, **116**, p 332–342.
28. U. Sunkari, S.R. Reddy, B.D.S. Rathod, D. Kumar, R. Saha, S. Chatterjee and P.P. Bhattacharjee, Tuning Nanostructure Using Thermo-Mechanical Processing for Enhancing Mechanical Properties of Complex Intermetallic Containing $\text{CoCrFeNi}_{2.1}\text{Nbx}$ High Entropy Alloys, *Mater. Sci. Eng. A*, 2020, **769**, p 138489.
29. X.H. Chen, W.Y. Xie, J. Zhu, Z.D. Wang, Y.L. Wang and Y.F. Ma, Influences of Ti Additions on the Microstructure and Tensile Properties of $\text{AlCoCrFeNi}_{2.1}$ Eutectic High Entropy Alloy, *Intermetallics*, 2021, **128**, p 107024.
30. H. Zhu, C.T. Liu, L.M. Pike and P.K. Liaw, Enthalpies of Formation of Binary Laves Phases, *Intermetallics*, 2002, **10**, p 579–595.

31. T.T. Xu, Y.P. Lu, Z.Q. Cao, T.M. Wang and T.J. Li, Effects of Ta Addition on the Microstructure and Mechanical Properties of CoCu_{0.5}FeNi High-Entropy Alloy, *J. Mater. Eng. Perform.*, 2019, **28**(6), p 7642–7648.
32. L. Jiang, Y.P. Lu, Y. Dong, T.M. Wang, Z.Q. Cao and T.J. Li, Effects of Nb Addition on Structural Evolution and Properties of the CoFeNi₂V_{0.5} High-Entropy Alloy, *Appl. Phys. A Mater.*, 2015, **119**(1), p 291–297.
33. Y. Zhang, Y.J. Zhou, J.P. Lin, G.L. Chen and P.K. Liaw, Solid-Solution Phase Formation Rules for Multi-Component Alloys, *Adv. Eng. Mater.*, 2008, **10**, p 534–538.
34. S. Guo and C.T. Liu, Phase Stability in High Entropy Alloys: Formation of Solid-Solution Phase or Amorphous Phase, *Prog. Nat. Sci. Mater. Int.*, 2011, **21**, p 433–446.
35. B. Chanda and J. Das, An Assessment on the Stability of the Eutectic Phases in High Entropy Alloys, *J. Alloy. Compd.*, 2019, **798**, p 167–173.
36. M.G. Poletti and L. Battezzati, Electronic and Thermodynamic Criteria for the Occurrence of High Entropy Alloys in Metallic Systems, *Acta Mater.*, 2014, **75**, p 297–306.
37. Y. Dong, Y.P. Lu, L. Jiang, T.M. Wang and T. Li, Effects of Electro-Negativity on the Stability of Topologically Close-Packed Phase in High Entropy Alloys, *Intermetallics*, 2014, **52**, p 105–109.
38. S. Guo, C. Ng, J. Lu and C.T. Liu, Effect of Valence Electron Concentration on Stability of fcc or bcc Phase in High Entropy Alloys, *J. Appl. Phys.*, 2011, **109**(10), p 103505.
39. Y.M. Tan, J.S. Li, J. Wang, M. Kolbe and H.C. Kou, Microstructure Characterization of CoCrFeNiMnPdx Eutectic High-Entropy Alloys, *J. Alloy. Compd.*, 2018, **731**, p 600–611.
40. F. He, Z.J. Wang, P. Cheng, Q. Wang, J.J. Li, Y.Y. Dang, J.C. Wang and C.T. Liu, Designing Eutectic High Entropy Alloys of CoCrFeNiNbx, *J. Alloy. Compd.*, 2016, **656**, p 284–289.
41. Y. Guo, L. Liu, Y. Zhang, J.G. Qi, B. Wang, Z.F. Zhao, J. Shang and J. Xiang, A Superfine Eutectic Microstructure and the Mechanical Properties of CoCrFeNiMox High-Entropy Alloys, *J. Mater. Res.*, 2018, **33**, p 3258–3265.
42. W.Y. Huo, H. Zhou, F. Fang, X.F. Zhou, Z.H. Xie and J.Q. Jiang, Microstructure and Properties of Novel CoCrFeNiTax Eutectic High-Entropy Alloys, *J. Alloy. Compd.*, 2018, **735**, p 897–904.
43. X.Z. Gao, Y.P. Lu, B. Zhang, N.N. Liang, G.Z. Wu, G. Sha, J.Z. Liu and Y.H. Zhao, Microstructural Origins of High Strength and High Ductility in an AlCoCrFeNi_{2.1} Eutectic High-Entropy Alloy, *Acta Mater.*, 2017, **141**, p 59–66.
44. Z.Z. Niu, Y.Z. Wang, C. Geng, J. Xu and Y. Wang, Microstructural Evolution, Mechanical and Corrosion Behaviors of as-annealed CoCrFeNiMox (x = 0, 0.2, 0.5, 0.8, 1) High Entropy Alloys, *J. Alloy. Compd.*, 2019, **820**, p 153273.
45. W.P. Li, X.G. Wang, B. Liu, Q.H. Fang and C. Jiang, Fracture Mechanisms of a Mo Alloyed CoCrFeNi High Entropy Alloy: In-situ SEM Investigation, *Mater. Sci. Eng. A*, 2018, **723**, p 79–88.
46. U. Sunkari, R.R. Seelam, K.S. Athira, S. Chatterjee and P.P. Bhattacharjee, Effect of Niobium Alloying on the Microstructure, Phase Stability and Mechanical Properties of CoCrFeNi_{2.1}Nbx High Entropy Alloys: Experimentation and Thermodynamic Modelling, *Mater. Sci. Eng. A*, 2020, **793**, p 139897.
47. U. Sunkari, S.R. Reddy, B.D.S. Rathod, S.S. Sathesh Kumar, R. Saha, S. Chatterjee and P.P. Bhattacharjee, Heterogeneous Precipitation Mediated Heterogeneous Nanostructure Enhances Strength-Ductility Synergy in Severely Cryo-Rolled and Annealed CoCrFeNi_{2.1}Nb_{0.2} High Entropy Alloy, *Sci. Rep.*, 2020, **10**, p 1–9.
48. W.H. Liu, J.Y. He, H.L. Huang, H. Wang, Z.P. Lu and C.T. Liu, Effects of Nb Additions on the Microstructure and Mechanical Property of CoCrFeNi high-Entropy Alloys, *Intermetallics*, 2015, **60**, p 1–8.

Publisher's Note Springer Nature remains neutral with regard to jurisdictional claims in published maps and institutional affiliations.